

# Safe Planning in Unknown Environments using Conformalized Semantic Maps

David Smith Sundarsingh<sup>1</sup>, Yifei Li<sup>1</sup>, Tianji Tang<sup>2</sup>, George J. Pappas<sup>3</sup>, Nikolay Atanasov<sup>2</sup> and Yiannis Kantaros<sup>1</sup>

**Abstract**—This paper addresses semantic planning problems in unknown environments under perceptual uncertainty. The environment contains multiple unknown semantically labeled regions or objects, and the robot must reach desired locations while maintaining class-dependent distances from them. We aim to compute robot paths that complete such semantic reach-avoid tasks with user-defined probability despite uncertain perception. Existing planning algorithms either ignore perceptual uncertainty—thus lacking correctness guarantees—or assume known sensor models and noise characteristics. In contrast, we present the first planner for semantic reach-avoid tasks that achieves user-specified mission completion rates without requiring any knowledge of sensor models or noise. This is enabled by quantifying uncertainty in semantic maps—constructed on-the-fly from perceptual measurements—using conformal prediction in a model- and distribution-free manner. We validate our approach and the theoretical mission completion rates through extensive experiments, showing that it consistently outperforms baselines in mission success rates.

## I. INTRODUCTION

Autonomous robot navigation has received considerable research attention, leading to the development of numerous planners capable of designing trajectories that reach known goal regions while maintaining safe distances from obstacles [1]–[3]. Recent advances in AI-enabled robot vision and semantic mapping have created new opportunities to move beyond these well-studied geometric planning approaches toward semantic planning, where task completion requires reasoning not only about the geometric structure of the environment (e.g., obstacle locations) but also its semantic structure (e.g., object categories or terrain types) [4], [5].

This paper focuses on semantic planning problems in environments populated with multiple objects and regions whose locations and semantic categories are initially unknown. The robot’s goal is to reach desired destinations while maintaining category-dependent safety distances from these semantic regions and objects. Recent planning algorithms tackle such tasks by leveraging AI-enabled perception systems (e.g., segmentation and object recognition algorithms) to collect geometric and semantic observations [6]–[17]. These approaches typically either (i) employ deep learning methods to directly map perceptual inputs to robot actions (e.g., [14], [15], [17])

<sup>1</sup>The authors are with Department of Electrical and Systems Engineering, Washington University in St Louis, MO, 63108, USA. Emails: {d.s.sundarsingh,liyifei,ioannisk}@wustl.edu.

<sup>2</sup>The authors are with Department of Electrical and Computer Engineering at University of California, San Diego, CA, 92093, USA. Emails: {tit006,natanasov}@ucsd.edu.

<sup>3</sup>The author is with the Department of Electrical and Systems Engineering, University of Pennsylvania, Philadelphia, PA 19104, USA. Emails: pappasg@seas.upenn.edu.

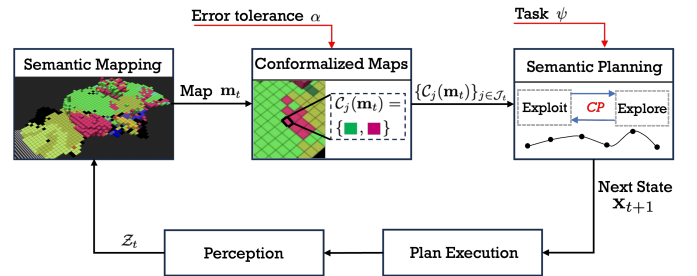


Fig. 1. Illustration of the proposed planning framework for semantic reach-avoid tasks  $\psi$ . Given categorical and range measurements, a semantic map is constructed [19]. To account for map uncertainty caused by perceptual imperfections, conformal prediction is employed to generate sets of maps that contain the ground-truth environment with a user-defined probability. These sets are then used by a planner to generate uncertainty-aware paths that complete the assigned tasks with a user-defined probability  $1 - \alpha$ .

or (ii) leverage semantic SLAM techniques [18]–[20] to build semantic maps that are used by downstream planners (e.g., [6], [7], [21]). Despite impressive empirical performance, in these architectures the planning layer generally treats outputs from the perception or mapping modules as ground truth, ignoring their inherent uncertainty. As a result, these approaches lack mission completion guarantees. Attempts to model perceptual uncertainty within semantic and geometric planning have been investigated in [6], [7], [22] and [23]–[27], respectively. However, these methods often depend on unreliable proxies such as SLAM-derived confidence scores, or assume known sensor models and Gaussian noise—assumptions that may not hold in practice. Specifically: (i) SLAM-based uncertainty metrics often stem from fusing uncalibrated confidence scores from perception systems [28]; (ii) sensor models are often nonlinear and poorly characterized in real environments; and (iii) noise is often non-Gaussian or multi-modal.

This paper addresses these limitations by developing a semantic planner for unknown environments that completes semantic reach-avoid tasks with a user-defined probability under perceptual uncertainty, while remaining agnostic to sensor models and noise characteristics. Robots are equipped with imperfect perception systems (e.g., cameras with semantic segmentation) that provide geometric and semantic observations. Our framework consists of three main components; see Fig. 1. First, we leverage existing semantic mapping algorithms that capture dense semantic and geometric environmental information and generate a multi-class semantic map of the environment [19]. Second, we quantify uncertainty of the generated semantic maps using Conformal Prediction (CP), a statistical, model- and distribution-free tool [29]. This produces a set of maps guaranteed to contain the ground truth with a user-defined probability. Third, we develop a semantic planner that balances exploitation and exploration. In

exploitation mode, the planner selects the most conservative map from the CP set and generates paths using any search- or sampling-based planner [1]–[3]. When uncertainty is too high for a feasible solution to exist, the planner switches to exploration mode to reduce uncertainty (modeled by the size of the CP set) until a feasible path can be found. We show both theoretically and empirically that our method achieves desired mission completion rates. We also conduct experiments highlighting the exploitation–exploration trade-offs as the required success probability increases. Our comparative experiments also demonstrate that our approach outperforms baselines that either treat mapping outputs as ground truth or rely on uncertainty metrics provided by the mapping algorithm.

**Related Work:** (i) *Perception-based Planning:* As discussed earlier, numerous planners for unknown environments have been proposed. However, these either neglect perceptual/mapping uncertainty and, thus, lack correctness guarantees [8]–[17], or assume known sensor models and noise characteristics to design probabilistically correct paths [6], [7], [23]–[27]. In contrast, our planner achieves user-specified mission completion rates without assuming any knowledge of sensor models or noise. The closest work to ours is [30], which employs CP to quantify the uncertainty of object detectors and design probabilistically correct paths. However, [30] focuses solely on geometric planning and cannot straightforwardly handle combined geometric and semantic uncertainty. (ii) *CP for Verified Autonomy:* CP has recently been applied to quantify the uncertainty of various AI-enabled components to ensure verified autonomy; see the survey in [31]. Applications include trajectory prediction models [32], [33], large language models [34], [35], decision-making algorithms [36], image classifiers [37], diffusion dynamic models [38], and 3D human pose estimators [39]. Inspired by these works, we propose the first use of CP to quantify semantic map uncertainty, thereby enabling probabilistically correct semantic planning.

**Contributions:** The contributions of this paper can be summarized as follows. First, we introduce the first semantic planner for unknown environments that achieves user-defined mission completion rates under perceptual uncertainty, while remaining agnostic to sensor models and noise characteristics. Second, we present the first application of CP to quantify the uncertainty of semantic maps generated by existing mapping algorithms, also in a model-agnostic manner. Third, we present experiments that validate the theoretical mission completion guarantees and show that our method consistently outperforms baselines in terms of mission success rates.

## II. PROBLEM STATEMENT

### A. Robot & Environment Modeling

Consider a robot with configuration  $\mathbf{x}_t \in \mathcal{X}$  at discrete time  $t \geq 0$ . We assume that the configuration  $\mathbf{x}_t$  is known (e.g., from encoders and localization). The robot operates in an environment  $\Omega \subseteq \mathbb{R}^d$ ,  $d \in \{2, 3\}$ , which is represented as a collection of disjoint sets  $\mathcal{L}_k \subseteq \Omega$ , each associated with a semantic category  $k \in \mathcal{K} = \{0, 1, \dots, K\}$  (e.g., cars, walls, trees). Here,  $\mathcal{L}_0$  denotes free space, and  $\mathcal{L}_k$  are fixed over time and unknown to the robot.

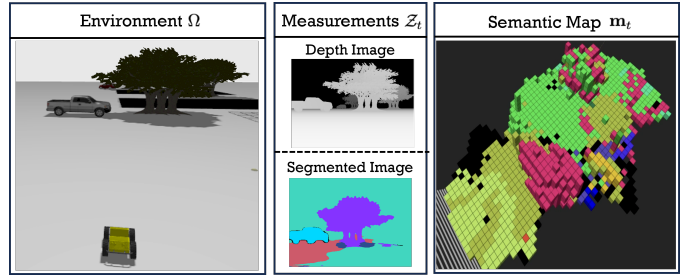


Fig. 2. The mapping algorithm uses depth and categorical measurements  $\mathcal{Z}_t$ , provided as a depth image and a segmented image, respectively, to generate a 3D semantic grid map  $\mathbf{m}_t$ . Each grid cell is associated with a semantic category, and its color corresponds to that category.

### B. Reachability Task with Semantic Safety Constraints

The robot is tasked with reaching a known set of goal states  $\mathcal{X}_g \subseteq \mathcal{X}$  while maintaining class-dependent safe distances  $d_k$  from regions  $\mathcal{L}_k$ . We denote the assigned task by  $\psi$ . As an example, consider a safety specification requiring the robot to maintain a distance of 1m from  $\mathcal{L}_{\text{tree}}$  and 3m from  $\mathcal{L}_{\text{car}}$  while navigating towards a desired destination. Such semantic reach-avoid tasks can be completed by following a finite-horizon path  $\mathbf{x}_{0:H}$ , defined as a sequence of robot states, i.e.,  $\mathbf{x}_{0:H} = \mathbf{x}_0, \dots, \mathbf{x}_t, \dots, \mathbf{x}_H$ , for some horizon  $H$ , where (i)  $\mathbf{x}_H \in \mathcal{X}_g$ , and (ii) all  $\mathbf{x}_t$  satisfy the safety constraints, i.e.,

$$\min_{\mathbf{q} \in \mathcal{L}_k} \|\mathbf{x}_t|_{\Omega} - \mathbf{q}\|_2 \geq d_k, \quad \forall t \in \{0, \dots, H\}, \quad (1)$$

for all  $\mathcal{L}_k \subseteq \Omega$ , where  $k \in \mathcal{K} \setminus \{0\}$ . In (1),  $\mathbf{x}_t|_{\Omega}$  denotes the robot’s position, i.e., the projection of the robot state onto  $\Omega$ . Completion of  $\psi$  using a robot path  $\mathbf{x}_{0:H}$  is denoted by  $\mathbf{x}_{0:H} \models \psi$ , where  $\models$  denotes the satisfaction relation.

### C. Perception System and Semantic Mapping

The robot is equipped with a sensor of range  $r_{\max} > 0$  that provides information about the distances to, and semantic categories of, surrounding objects along a set of rays. We denote by  $\mathcal{Z}_t := \{z_{t,b}\}_b$  the set of measurements collected along ray  $b$  at time  $t$ , where each measurement is given by  $z_{t,b} = \{r_{t,b}, y_{t,b}\}$ , with  $r_{t,b} \in \mathbb{R}_{\geq 0}$  and  $y_{t,b} \in \mathcal{K}$  denoting the range and categorical measurements, respectively. Such information can be obtained by processing RGB-D images using a semantic segmentation algorithm [40]; see Fig. 2.

These labeled range measurements can be fused online to build a semantic representation of  $\Omega$  using existing semantic mapping algorithms. In particular, we adopt [19], which models the environment as a multi-class grid map  $\mathbf{m}$  defined as a collection of cells  $j \in \mathcal{J} = \{1, \dots, M\}$ , each labeled with a category  $m_j \in \mathcal{K}$  and represented by its center  $c_j \in \Omega$ ; see Fig. 2. To account for perceptual noise, each cell  $m_j$  maintains a probability mass function (PMF)  $p_t(m_j) = p(m_j | \mathbf{x}_{0:t}, \mathcal{Z}_{0:t})$  over  $\mathcal{K}$ , conditioned on the measurements  $\mathcal{Z}_{0:t}$  collected along the robot path  $\mathbf{x}_{0:t}$ . If at some  $t$ , no measurement corresponds to cell  $j$ ,  $p_t(m_j) = p_{t-1}(m_j)$ . Accordingly, the distribution of map is defined as  $p_t(\mathbf{m}) = \prod_{j \in \mathcal{J}} p_t(m_j)$  [19]. For brevity, we denote by  $\sigma$  a mapping algorithm that takes as input the distributions  $p_{t-1}(m_j)$  and the new measurement  $\mathcal{Z}_t$  collected at  $\mathbf{x}_t$ , and outputs the updated distributions  $p_t(m_j)$  for all  $j \in \mathcal{J}_t$ , i.e.,  $p_t(\mathbf{m}) = \sigma(\Omega, p_{t-1}(\mathbf{m}), \mathcal{Z}_t)$ , where  $\mathcal{J}_t \subseteq \mathcal{J}$  is

the set of indices of the grid cells that have been detected till time  $t$ ; map update at  $t = 0$  occurs using a prior  $p_{-1}(\mathbf{m})$ . Hereafter, when it is clear from the context, we refer to the random variable  $\mathbf{m}_t$  without explicitly specifying its density  $p_t(\mathbf{m})$ .

#### D. Problem Statement

We assume that mission scenarios  $\xi = (\mathbf{x}_0, \Omega, \psi)$ , determined by the initial robot state  $\mathbf{x}_0$ , an environment  $\Omega$ , and a semantic reach-avoid task  $\psi$ , are sampled from an unknown distribution  $\mathcal{D}$ . While  $\mathcal{D}$  is unknown, we assume that i.i.d. scenarios  $\xi$  can be sampled from it. As discussed above the robot does not know  $\Omega$ ; instead it has access to a prior map  $\mathbf{m}_{-1}$  that can be updated online using the mapping algorithm  $\sigma$ . We aim to design a planning algorithm that, given a scenario sampled from  $\mathcal{D}$ , can generate a robot path  $\mathbf{x}_{0:H}$ , for some  $H > 0$ , that completes  $\psi$  with a user-specified probability  $1 - \alpha$ , given the sequence of maps  $\mathbf{m}_{0:H}$  updated online. In summary, we address the following problem:

**Problem II.1.** Consider a mission scenario  $\xi = (\mathbf{x}_0, \Omega, \psi) \sim \mathcal{D}$ , where  $\Omega$  is unknown but prior information  $\mathbf{m}_{-1}$  is available. Given a mapping algorithm  $\sigma$ , design a planning algorithm that generates a robot path  $\mathbf{x}_{0:H}$ , for some  $H > 0$ , ensuring that

$$\mathbb{P}_{\xi \sim \mathcal{D}}(\mathbf{x}_{0:H} \models \psi \mid \mathbf{m}_{0:H}) \geq 1 - \alpha, \quad (2)$$

where and  $1 - \alpha \in (0, 1)$  is a user-specified success rate.

We note that the probabilistic task completion statement in (2) accounts for errors at the mapping level, but not necessarily at the sensor level. For instance, certain sensor rays  $b$  may fail to return a measurement from an object occupying cell  $j$  (e.g., due to malfunctions). In such cases, the PMF of  $m_j$  is never updated, creating the false impression that it lies in free space. The guarantee in (2) does not cover these sensor-level errors; rather, it addresses labeling and mapping errors in cells  $m_j$  for which at least one associated measurement has been collected. Failures can also occur due to objects that (i) are close enough to the robot, leading to violations of (1) but they (ii) lie outside the sensor's field of view. To exclude such sensor-based errors, we make the following assumption.

**Assumption II.2** (Sensors). (i) The robot is equipped with an omnidirectional sensor of range  $r_{max}$  generating  $\mathcal{Z}_t$ . (ii) The sensor range  $r_{max}$  satisfies  $r_{max} \geq d_k$  for all  $k \in \mathcal{K}$  (iii) If a cell  $j$  in the map is occupied by an object lying within the sensor's field of view, a measurement associated with it will always be returned. Due to (iii), we have that if no measurements are obtained for a cell  $j$  (lying within the sensor range), then it corresponds to free-space.

### III. SAFE SEMANTIC PLANNING IN UNKNOWN ENVIRONMENTS

A natural approach to Problem II.1 is to plan directly over the distribution of the map  $\mathbf{m}_t$ , as in [6], [7]. However, in practice, the sensor models used to update the map distribution are inaccurate, so the PMFs  $p_t(m_j)$  do not represent true

probabilities. As a result, planning directly over  $\mathbf{m}_t$  may compromise the probabilistic correctness of the generated paths. To overcome this limitation, we propose a new planner that makes no assumptions about the sensor model and noise characteristics. In Section III-A, we employ conformal prediction (CP) to 'calibrate'  $\mathbf{m}_t$  by computing prediction sets for each cell  $j \in \mathcal{J}_t$  that contain the true label with user-defined confidence. These sets are then used in Section III-B to design paths  $\mathbf{x}_{0:H}$  that solve Problem II.1.

#### A. Conformalizing Semantic Maps

As discussed earlier, the distribution of  $\mathbf{m}_t$  does not represent true probabilities compromising the correctness of paths designed only using  $\mathbf{m}_t$ . To address this, for any test scenario  $\xi_{test} \sim \mathcal{D}$  associated with an unknown environment  $\Omega$ , we aim to design sets  $\mathcal{C}_j(\mathbf{m}_t) \subseteq \mathcal{K}$  of labels for each cell  $j \in \mathcal{J}_t$  detected along a path  $\mathbf{x}_{0:H}$  and time step  $t \in \{0, \dots, H\}$  satisfying the following property:

$$\mathbb{P}_{\xi \sim \mathcal{D}}(C_{0:H} \mid \mathbf{m}_{0:H}) \geq 1 - \alpha, \quad (3)$$

where  $C_{0:H} = \bigwedge_{j \in \mathcal{J}_t, t \in [0:H]} (k_j^{gt} \in \mathcal{C}_j(\mathbf{m}_t))$  and  $k_j^{gt} \in \mathcal{K}$  is the true label of the region occupying cell  $j$ . In words, (3) guarantees that, with probability at least  $1 - \alpha$ , the sets  $\mathcal{C}_j(\mathbf{m}_t)$  contain the true labels  $k_j^{gt}$  for all cells  $j \in \mathcal{J}_t$  in  $\mathbf{m}_t$ , all time steps  $t \in \{0, \dots, H\}$ , and any robot path  $\mathbf{x}_{0:H}$  followed to construct  $\mathbf{m}_{0:H}$ .

To construct these sets for  $\xi_{test}$ , we employ CP to quantify uncertainty in the outputs of the mapping algorithm  $\sigma$ . Applying CP requires (i) a set of calibration mission scenarios  $\{\xi_i = (\mathbf{x}_{0,i}, \Omega_i, \psi_i)\}_{i=1}^D$  drawn from  $\mathcal{D}$  with known ground-truth labels  $k_j^{gt}$  for all  $j \in \mathcal{J}$ , and (ii) a non-conformity score (NCS) that captures the error of  $\sigma$ , which generates maps  $\mathbf{m}_{0:H}$  along any path  $\mathbf{x}_{0:H}$ . It is crucial that the NCS accounts for mapping errors along arbitrary robot paths, rather than a single fixed path, since otherwise (3) would hold only for that path. Thus, we adopt the following NCS, which is path-agnostic (and, consequently, task-agnostic) and captures the worst-case mapping error, associated with the calibration mission scenario  $\xi_i$ :

$$s_i = \max_{\mathbf{x}_{0:H} \in \mathcal{P}; j \in \mathcal{J}_t; t \in [0,H]} \left(1 - p_t(m_j = k_j^{gt})\right), \quad (4)$$

where  $\mathcal{P}$  is the set of all possible finite paths in the calibration environment  $\Omega_i$ . In (4), the term  $p_t(m_j = k_j^{gt})$  denotes the probability that cell  $j$  has the ground-truth label according to the map  $\mathbf{m}_t$ . Consequently,  $1 - p_t(m_j = k_j^{gt})$  models the mapping error at cell  $j$  after collecting measurements along a specific path  $\mathbf{x}_{0:t}$ . The maximum operator in (4) computes the worst-case error, i.e., the largest error across all cells  $j \in \mathcal{J}_t$ , all time steps  $t \in [0, H]$ , and all paths  $\mathbf{x}_{0:H} \in \mathcal{P}$ .<sup>1</sup> We compute the NCSs  $\{s_i\}_{i=1}^D$  for all calibration scenarios and determine their  $\frac{[(D+1)(1-\alpha)]}{D}$ -quantile, denoted by  $\hat{s}$ .

<sup>1</sup>Computing (4) exactly requires evaluating the maximum over an infinite number of paths, which is impractical. As in [30], in practice the NCS is approximated using a finite set of paths  $\mathcal{P}$ ; see Section V-C for details.

**Algorithm 1** Conformalization of Semantic Map

---

```

1: Input: Map  $\mathbf{m}_t$ , score quantile  $\hat{s}$ , semantic classes  $\mathcal{K}$ 
2: for  $j \in \mathcal{J}_t$  do
3:    $C_j(\mathbf{m}_t) = \{k \in \mathcal{K} | p_t(m_j = k) \geq 1 - \hat{s}\}$ 
return  $\{C_j(\mathbf{m}_t)\}_{j \in \mathcal{J}_t}$ 

```

---

For an unseen/test mission scenario  $\xi_{\text{test}} \sim \mathcal{D}$  with unknown true labels for cells  $j$ , at each step  $t$  we compute the following prediction set of labels for all cells  $j \in \mathcal{J}_t$  (see Alg. 1):

$$C_j(\mathbf{m}_t) = \{k \in \mathcal{K} | p_t(m_j = k) \geq 1 - \hat{s}\}, \quad (5)$$

collecting all labels  $k \in \mathcal{K}$  satisfying  $p_t(m_j = k) \geq 1 - \hat{s}$  where  $p_t$  refers to the PMF computed by  $\sigma$  [line 3, Alg. 1]. In Section IV, we show that these prediction sets satisfy (3).

*B. Planning over Conformalized Semantic Maps*

Consider a mission scenario  $\xi = (\mathbf{x}_0, \Omega, \psi)$  drawn from  $\mathcal{D}$ . Our goal is to compute a plan  $\mathbf{x}_{0:H}$  satisfying  $\psi$  with probability at least  $1 - \alpha$ . This path will be constructed incrementally as the map  $\mathbf{m}_t$  is updated online; see Alg. 2. First, we collect the calibration dataset  $\{\xi_i\}_{i=1}^D$ , and compute  $\hat{s}$  as described in Section III-A [lines 3-4, Alg. 2]. Assume that at time  $t > 0$ , the robot is at state  $\mathbf{x}_t$ , collects measurements  $\mathcal{Z}_t$ , and constructs the map  $\mathbf{m}_t$  [lines 6-7, Alg. 2]. Using  $\mathbf{m}_t$ , the prediction sets  $C_j(\mathbf{m}_t)$  are constructed for all cells  $j \in \mathcal{J}_t$  [line 8, Alg. 2]. We now discuss how the next robot state  $\mathbf{x}_{t+1}$  is computed using these sets [lines 9–14, Alg. 2]. The next state  $\mathbf{x}_{t+1}$  must be chosen so that it satisfies (1). Since the regions  $\mathcal{L}_k$  are unknown, satisfaction of (1) must be checked using the map  $\mathbf{m}_t$ . Specifically, given  $\mathbf{m}_t$ , (1) can be re-written as:

$$\|\mathbf{x}_{t+1} | \Omega - c_j\| \geq d_{k_j} + r_m, \quad (6)$$

for all cells  $j \in \mathcal{J}_t$ , where  $r_m$  is the grid resolution,  $c_j \in \Omega$  is the center of cell  $j$  and  $k_j$  is the label assigned to cell  $j$ .<sup>2</sup> Note that cells  $j \in \mathcal{J} \setminus \mathcal{J}_t$  within the sensor range  $r_{\text{max}}$  are free space due to Assumption II.2. The next state  $\mathbf{x}_{t+1}$  can be chosen using any existing planner if the true label  $k_j^{\text{gt}}$  of each cell  $j$  were known to the robot, which is not the case here. To address this, we leverage sets  $C_j(\mathbf{m}_t)$ , constructed as shown in (5), that contain the true label with user-defined confidence. From each set, we select the most conservative label, i.e.,  $k_j = \arg\max_{k \in C_j(\mathbf{m}_t)} d_k$ , for every cell  $j \in \mathcal{J}_t$ . All cells  $j \in \mathcal{J} \setminus \mathcal{J}_t$  outside the sensor range are considered part of the free space i.e.,  $k_j = 0$ , for all  $j \in \mathcal{J} \setminus \mathcal{J}_t$ . Given this assignment of labels, the planner adaptively switches between exploitation and exploration modes as follows.

**Exploitation Phase:** Using an existing motion planner [1]–[3], we first check whether there exists a robot path  $\mathbf{p} = \mathbf{p}_0, \mathbf{p}_1, \dots, \mathbf{p}_T$ , with  $\mathbf{p}_n \in \mathcal{X}$  for all  $n \in \{0, \dots, T\}$  and some  $T \geq 0$  that completes  $\psi$  under the assigned labels  $k_j$  [line 9, Alg. 2]. The path must satisfy  $\mathbf{p}_0 = \mathbf{x}_t$ ,  $\mathbf{p}_T \in \mathcal{X}_g$ , and  $\|\mathbf{p}_n | \Omega - c_j\| \geq d_{k_j} + r_m$  for all  $n$ . If such a feasible plan exists, the robot selects  $\mathbf{x}_{t+1} = \mathbf{p}_1$  and moves towards it, updates the time step to  $t + 1$ , and repeats the process [lines 12-14, Alg. 2].

<sup>2</sup>The grid resolution is added to ensure that the robot never gets close to an object even if the object occupies the entirety of the grid cell.

**Algorithm 2** Safe Planning Over Conformalized Maps

---

```

1: Input: Prior map  $\mathbf{m}_{-1}$ ; Task  $\psi$ ; Initial state  $\mathbf{x}_0$ ; Set of labels  $\mathcal{K}$ 
2: Initialize  $t = 0$ 
3: Collect calibration mission scenarios  $\{\xi_i\}_{i=1}^D$ 
4: Compute NCSs  $\{s_i\}_{i=1}^D$  and quantile  $\hat{s}$ 
5: while  $\mathbf{x}_t \notin \mathcal{X}_g$  do
6:    $\mathcal{Z}_t = \text{Measure}(\Omega, \mathbf{x}_t)$ 
7:    $\mathbf{m}_t = \sigma(\Omega, \mathbf{m}_{t-1}, \mathcal{Z}_t)$ 
8:    $\{C_j(\mathbf{m}_t)\}_{j \in \mathcal{J}_t} = \text{Conformalize}(\mathbf{m}_t, \hat{s}, \mathcal{K})$  (see Alg. 1)
9:    $\mathbf{p} = \text{Plan}(\mathbf{x}_t, \mathcal{X}_g, \{C_j(\mathbf{m}_t)\}_{j \in \mathcal{J}_t})$ 
10:  if  $\mathbf{p} = \emptyset$  then
11:     $\mathbf{p} = \text{Explore}(\mathbf{x}_t, \{C_j(\mathbf{m}_t)\}_{j \in \mathcal{J}_t})$ 
12:   $\mathbf{x}_{t+1} = \mathbf{p}(1)$ 
13:   $\text{Execute}(\mathbf{x}_{t+1})$ 
14:   $t = t + 1$ 

```

---

**Exploration Phase:** If no feasible solution is found during the exploitation phase, the planner switches to exploration [line 10, Algo. 2]. In this mode, any exploration algorithm can be employed to generate paths  $\mathbf{p}$  that optimize information-theoretic objectives (e.g., mutual information) subject to the constraints in (6); see, e.g., [19], [41]. Given such a path  $\mathbf{p}$ , the planner selects  $\mathbf{x}_{t+1} = \mathbf{p}(1)$ , sends it to the robot, updates the time step to  $t + 1$ , and repeats the process [lines 9-14, Alg. 2]. The goal is for exploration paths to reduce uncertainty (i.e., the size of the prediction sets) sufficiently for the robot to re-enter exploitation mode and eventually complete  $\psi$ .

During both exploration and exploitation we also ensure that  $\|\mathbf{x}_{t+1} - \mathbf{x}_t\| < r_{\text{max}}$  to eliminate cases where the next state may lie in the unexplored part of the map. The above process terminates once  $\mathbf{x}_{t+1} \in \mathcal{X}_g$ . Concatenation of these states across time yields  $\mathbf{x}_{0:H}$ .

## IV. PERFORMANCE GUARANTEES

In this section, we show that our planner addresses Problem II.1, i.e., the path  $\mathbf{x}_{0:H}$  generated by Algorithm 2 completes  $\psi$  with probability  $1 - \alpha$ . This result builds upon the fact that the sets  $C_j(\mathbf{m}_t)$ , constructed by Alg. 1, satisfy (3), i.e., they jointly contain the true labels for all  $j \in \mathcal{J}_t$ ,  $t \in [0, H]$  and any path  $\mathbf{x}_{0:H}$  with probability at least  $1 - \alpha$ . This property is shown in the following proposition.

**Proposition IV.1** (Mapping Guarantees). *Consider a test scenario  $\xi_{\text{test}} = \{\mathbf{x}_{0,\text{test}}, \Omega_{\text{test}}, \psi_{\text{test}}\} \sim \mathcal{D}$  with unknown true labels  $\{k_j^{\text{gt}}\}_{j \in \mathcal{J}}$ . Given any path  $\mathbf{x}_{0:H}$  in  $\Omega_{\text{test}}$  yielding a sequence of maps  $\mathbf{m}_{0:H}$ , the prediction sets  $\{C_j(\mathbf{m}_t)\}_{j \in \mathcal{J}_t}$ , computed at every  $t \in \{0, \dots, H\}$  constructed by Alg. 1 satisfy (3), for a user-defined  $\alpha \in (0, 1)$ .*

*Proof.* Using a standard CP argument [30], [42], we have:

$$\mathbb{P}_{\xi_{\text{test}} \sim \mathcal{D}}(s_{\text{test}} \leq \hat{s} | \mathbf{m}_{0:H}) \geq 1 - \alpha, \quad (7)$$

where  $s_{\text{test}}$  is the NCS associated with  $\xi_{\text{test}}$ . Note that  $s_{\text{test}}$  is unknown as the ground truth labels  $k_j^{\text{gt}}$  for cells  $j$  are unknown. By definition of the NCS in (4), we have that  $s_{\text{test}} = \max_{\mathbf{x}_{0:H} \in \mathcal{P}, j \in \mathcal{J}_t, t \in [0:H]} 1 - p_t(m_j = k_j^{\text{gt}})$ . Plugging this into (7) yields the following result:

$$\mathbb{P}_{\xi_{\text{test}} \sim \mathcal{D}} \left( \max_{\mathbf{x}_{0:H} \in \mathcal{P}, j \in \mathcal{J}_t, t \in [0:H]} (1 - p_t(m_j = k_j^{\text{gt}})) \leq \hat{s} | \mathbf{m}_{0:H} \right) \geq 1 - \alpha.$$

Thus, for any path  $\mathbf{x}_{0:H} \in \mathcal{P}$ , we have that

$$\mathbb{P}_{\xi_{\text{test}} \sim \mathcal{D}} \left( \bigwedge_{\forall j \in \mathcal{J}_t, \forall t \in [0:H],} p_t(m_j = k_j^{\text{gt}}) \geq 1 - \hat{s} \mid \mathbf{m}_{0:H} \right) \geq 1 - \alpha. \quad (8)$$

Recall from (5) that the prediction sets  $\mathcal{C}_j(\mathbf{m}_t)$  collect all labels  $k \in \mathcal{K}$  satisfying  $p_t(m_j = k) \geq 1 - \hat{s}$ . Combining this with (8) results in (3), i.e.,  $\mathbb{P}_{\xi_{\text{test}} \sim \mathcal{D}} (C_{0:H} \mid \mathbf{m}_{0:H}) \geq 1 - \alpha$ , where  $C_{0:H} = \bigwedge_{\forall j \in \mathcal{J}_t, t \in [0:H]} (k_j^{\text{gt}} \in \mathcal{C}_j(\mathbf{m}_t))$ .  $\square$

Building on Proposition IV.1, we show that the path  $\mathbf{x}_{0:H}$  generated by Alg. 2 addresses Problem II.1. To show this result, we make the following assumptions about the exploration and planning algorithms employed in Alg. 2.

**Assumption IV.2.** (i) *The exploration algorithm can reduce mapping uncertainty—and, consequently, the size of the prediction sets—so that the planner eventually enters the exploitation mode. This implies that exploration is invoked only a finite number of times before a path  $\mathbf{x}_{0:H}$  is computed. This assumption guarantees that Alg. 2 eventually terminates with a path for any mission scenario  $\xi \sim \mathcal{D}$  and, therefore, mission failures cannot be attributed to inefficient exploration.* (ii) *The planning algorithm used in the exploitation phase is complete, i.e., if a feasible path  $\mathbf{p}$  exists that completes  $\psi$  under the assigned labels described in Section III-B, then the planner is guaranteed to find it. This assumption ensures that mission failures can only be attributed to mapping errors.*

**Theorem IV.3** (Planning Guarantees). *Given a test scenario  $\xi_{\text{test}} = \{\mathbf{x}_{0,\text{test}}, \Omega_{\text{test}}, \psi_{\text{test}}\} \sim \mathcal{D}$  with unknown true labels  $\{k_j^{\text{gt}}\}_{j \in \mathcal{J}}$ , Alg. 2 will generate a path  $\mathbf{x}_{0:H}$  satisfying (2).*

*Proof.* First, by Assumption IV.2, for any scenario  $\xi_{\text{test}} \sim \mathcal{D}$ , Algorithm 2 is guaranteed to terminate and return a path  $\mathbf{x}_{0:H}$ . Consequently, any failure to complete  $\psi$  can be attributed only to mapping errors.

Second, consider the path  $\mathbf{x}_{0:H}$  returned by Algorithm 2 for a scenario  $\xi_{\text{test}} \sim \mathcal{D}$ . We show that  $\mathbf{x}_{0:H}$  satisfies (2) by leveraging Proposition IV.1. Specifically, by construction of the exploration and exploitation modes in Algorithm 2, Assumption IV.2-(ii), and Assumption II.2 we have that: (i) all states  $\mathbf{x}_t$  in  $\mathbf{x}_{0:H}$  satisfy the imposed safety constraints given the labels  $k_j = \text{argmax}_{k \in \mathcal{C}_j(\mathbf{m}_t)} d_k$  assigned to cells  $j$ , i.e.,  $\max_{k \in \mathcal{C}_j(\mathbf{m}_t)} d_k + r_m \leq \|\mathbf{x}_{t+1} - c_j\|, \forall j \in \mathcal{J}_t$  and (ii)  $\mathbf{x}_H \in \mathcal{X}_g$ . Now, let us assume that the ground truth label is included in the prediction sets for all  $t \in \{0, \dots, H\}$ . This equivalently means that the probability that  $\mathbf{x}_{0:H}$  satisfies  $\psi$  with respect to the assigned labels, and implicitly the ground truth labels, is 1. The implicit satisfaction with respect to the ground truth is due to the consideration of the worst-case label in the prediction set that also contains the ground truth, In math, we express this as follows:

$$\mathbb{P}_{\xi_{\text{test}} \sim \mathcal{D}} (\mathbf{x}_{0:H} \models \psi \mid C_{0:H}, \mathbf{m}_{0:H}) = 1, \quad (9)$$

where  $C_{0:H} = \bigwedge_{\forall j \in \mathcal{J}_t, t \in [0:H]} (k_j^{\text{gt}} \in \mathcal{C}_j(\mathbf{m}_t))$ . Recall from Proposition IV.1, that  $\mathbb{P}_{\xi_{\text{test}} \sim \mathcal{D}} (C_{0:H} \mid \mathbf{m}_{0:H}) \geq 1 - \alpha$ . Combining this with (9) we get that  $\mathbf{x}_{0:H}$  satisfies (2).  $\square$

**Remark IV.4** (Dataset-conditional guarantees). *The guarantees in Proposition IV.1 and Theorem IV.3 are marginal, where the probabilities are over the randomness of the calibration set and the test scenario. A dataset-conditional guarantee which holds for a fixed calibration set across test scenarios can also be applied [43]. In such cases, Proposition IV.1 is modified such that with a probability of at least  $1 - \delta$  over the sampling of the calibration set  $\{\xi_i\}_{i=1}^D \sim \mathcal{D}$ ,  $\mathbb{P}_{\xi_{\text{test}} \sim \mathcal{D}} (C_{0:H} \mid \mathbf{m}_{0:H}, \{\xi_i\}_{i=1}^D) \geq \text{Beta}_{D+1-v,v}^{-1}(\delta)$ , where  $\text{Beta}_{D+1-v,v}^{-1}(\delta)$  is the  $\delta$ -quantile of the Beta distribution with parameters,  $D$  - the size of the calibration dataset, and  $v = \lfloor (D+1)\hat{\alpha} \rfloor$  and  $\hat{\alpha}$  is selected so that  $\text{Beta}_{D+1-v,v}^{-1}(\delta) \approx 1 - \alpha$ . Similarly, Theorem IV.3 is modified, where with a probability of at least  $1 - \delta$  over the sampling of the calibration dataset, we have that  $\mathbb{P}_{\xi_{\text{test}} \sim \mathcal{D}} (\mathbf{x}_{0:H} \models \psi \mid \mathbf{m}_{0:H}, \{\xi_i\}_{i=1}^D) \geq \text{Beta}_{D+1-v,v}^{-1}(\delta)$ .*

## V. EXPERIMENTAL VALIDATION

In this section, we present experiments to validate the proposed approach. Section V-A defines the robot model and the distribution  $\mathcal{D}$  used in our evaluation. Section V-B describes the configuration of the proposed algorithm and the evaluation metrics. The empirical performance of our method is presented in Section V-C, while Section V-D provides comparative results against uncertainty-informed and uncertainty-agnostic planners, showing that our approach outperforms the baselines in terms of mission completion rates. Finally, Section V-E reports success rates on out-of-distribution scenarios, highlighting potential failure cases. A video with an explanation of the framework, experiments and demonstrations can be found in [44].

### A. Setting Up Experiments: Robot & Distribution $\mathcal{D}$

**Robot:** Our experiments are conducted using ROS 2 Humble [45] and the Gazebo (Ignition) simulator. The simulated platform is a Clearpath Husky skid-steer ground vehicle with a maximum linear speed of 1.0 m/s and a maximum yaw rate of 0.5 rad/s. The robot is controlled at 2 Hz. It is equipped with a forward-facing RGB-D camera with a resolution of  $640 \times 480$ , a frame rate of 30 Hz, a horizontal FoV of  $90^\circ$ , a vertical FoV of  $73.7^\circ$ , and a sensing range of  $r_{\text{max}} = 10$  m. Note that this sensor is not omnidirectional, as required in Assumption II.2, due to its FoV; consequently, our algorithm is tested in a more challenging setting.

**Distribution  $\mathcal{D}$ :** The distribution  $\mathcal{D}$  is designed to generate mission scenarios  $\xi = \{\mathbf{x}_0, \Omega, \psi\}$  as follows. All environments  $\Omega$  have dimensions of  $70 \times 25$  m and contain objects from five semantic classes,  $\mathcal{K} = \{\text{person, car, truck, tree, free}\}$ . Specifically, each environment is populated with one car, one truck, one human, and three parallel rows of three trees. The tree locations remain fixed across all environments, while the car and truck are placed at randomized positions and orientations. The human position is also generated randomly, with a bias toward being placed near the trees. This choice enables testing our algorithm's performance in cases of partial occlusions. The initial robot location  $\mathbf{x}_0$  is selected randomly. The task  $\psi$  is

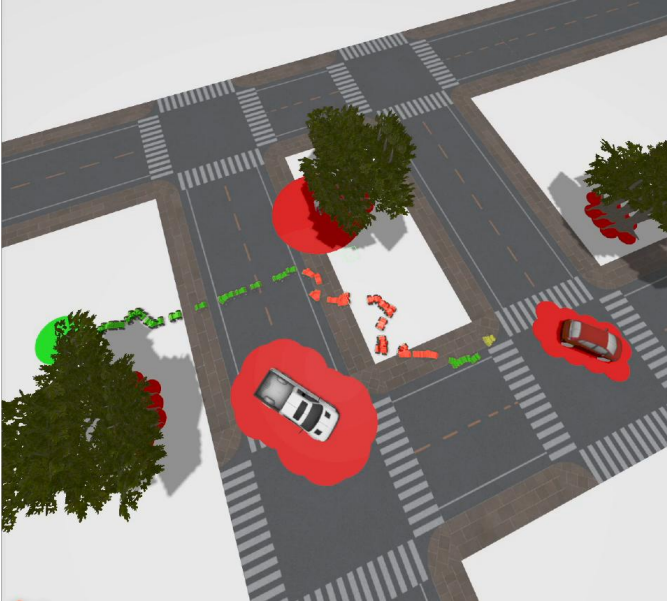


Fig. 3. Illustration of a path  $\mathbf{x}_{0:H}$  to the goal region (green disk) consisting of an exploration sub-path (red) and two exploitation sub-paths (green). The red regions model the unsafe regions as per (9).

designed so that the goal location is chosen randomly, and the class-based safety distances  $d_k$  in (9) are  $d_{\text{Person}} = 4$  m,  $d_{\text{Car}} = 1$  m,  $d_{\text{Truck}} = 2$  m, and  $d_{\text{Tree}} = 0.5$  m. An example mission scenario is shown in Figure 3.

### B. Setting Up the Proposed Planner & Evaluation Metrics

**Semantic Mapping:** To set up the semantic mapping algorithm introduced in [19], we use a Detectron2 model [46], trained on the COCO dataset [47], to semantically segment RGB images. The segmented outputs are fused over time to construct a 3D semantic octomap with resolution  $r_m = 1$  m. In our experiments, since we focus on a ground robot, we project this 3D map onto the X–Y plane, while considering height ranges relevant to the robot and ignoring objects that do not interfere with its motion; this gives rise to a 2D semantic class-based grid map. In doing so, we assume that no semantic objects are stacked vertically.

**Exploitation-Exploration:** The exploitation mode of Alg. 2 is implemented using a standard A\* search algorithm on the 2D grid map [1]. For exploration, we design an algorithm that randomly selects a next state  $\mathbf{x}_{t+1}$  near a voxel with a non-singleton prediction set subject to (6). This approach aims to decrease map uncertainty and specifically the size of prediction sets by driving the robot towards cell  $j$  with non-singleton sets. As discussed in Section III-B, however, any other exploration algorithm can be substituted.

**Conformalization of Maps:** Next, we discuss our implementation of the CP process described in Section III-A. Recall that the NCS in (4) requires evaluating the maximum over the set  $\mathcal{P}$ , which contains an infinite number of paths. Since this is impractical, following [30], we approximate the NCS using a finite subset  $\hat{\mathcal{P}} \subset \mathcal{P}$  consisting of 10 paths between the start and goal locations in a given calibration scenario  $\xi_j$ . Additionally, to avoid generating a new calibration dataset for every test scenario, we apply CP as described in Remark

IV.4, with  $\delta = 0.1$ . The value  $\hat{\alpha}$  is computed such that  $\text{Beta}_{D+1-v,v}^{-1}(\delta) \approx 1 - \alpha$ , and we then use  $\hat{\alpha}$  to compute the quantile  $\hat{s}$ . Our calibration dataset consists of 50 mission scenarios designed as discussed in Section V-A.

**Evaluation Metrics:** We consider four metrics. (i) The first metric is the *mapping success rate*, defined as  $S.R_{\text{map}} := \mathbb{1}(C_{0:H})$ , where  $C_{0:H} = \bigwedge_{j \in \mathcal{J}_t, t \in [0:H]} (k_j^{\text{gt}} \in \mathcal{C}_j(\mathbf{m}_t))$  and  $k_j^{\text{gt}}$  is the ground truth label of cell  $j$ . In words, for a given test scenario  $\xi_{\text{test}}$ ,  $S.R_{\text{map}} = 1$  if all constructed prediction sets  $\mathcal{C}_j(\mathbf{m}_t)$  contain the true labels  $k_j^{\text{gt}}$  for all  $j \in \mathcal{J}_t$  and  $t \in [0 : H]$ . Due to Proposition IV.1, the average mapping success rate of Alg. 2 across test scenarios drawn from  $\mathcal{D}$  is expected to be at least  $1 - \alpha$ . (ii) The second metric is the *mission success rate*, defined as  $S.R_{\text{mission}} := \mathbb{1}(\mathbf{x}_{0:H} \models \psi)$ . In words, for a given test scenario  $\xi_{\text{test}}$ ,  $S.R_{\text{mission}} = 1$  if the robot path  $\mathbf{x}_{0:H}$  satisfies the safety constraints in (9) and  $\mathbf{x}_H \in \mathcal{X}_g$ . Due to Theorem IV.3, the average mission success rate of Alg. 2 across test scenarios drawn from  $\mathcal{D}$  is expected to be at least  $1 - \alpha$ . (iii) The third metric is the *distance* traveled by the robot during deployment, which captures efficiency of the generated paths. (iv) The fourth metric is the *proportion of the overall path used for exploration*, quantifying how much of the trajectory was dedicated to reducing uncertainty in the environment.

### C. Empirical Evaluation of the Proposed Planner

We evaluate our proposed method for three user-defined success rates:  $1 - \alpha \in \{0.95, 0.9, 0.85\}$ . Specifically, we consider 61 test scenarios drawn from  $\mathcal{D}$  and report the average mapping and mission success rates as defined above. Additionally, we report the average path length and the average proportion of the path used for exploration, computed over all successful mission scenarios. The empirical results are reported in Table I. Observe that the empirical mapping success rates for  $1 - \alpha = 95\%$ ,  $90\%$  and  $85\%$  are  $93.36\%$ ,  $90.16\%$  and  $86.89\%$  respectively, validating Proposition IV.1. Now, it can be seen that for  $1 - \alpha = 0.95$ , the empirical mapping success rate is  $93.36\% < 95\%$ . Such small deviations are due to the finiteness of the calibration dataset, the number of paths that are considered for calibration, and the number of validation environments. For more information on the influence of finiteness on the empirical success rates, the readers are directed to [29]. In addition, the empirical mission success rates for  $1 - \alpha = 95\%$ ,  $90\%$ ,  $85\%$  are  $98.36\%$ ,  $96.72\%$ ,  $95.08\%$  respectively validating Theorem IV.3. Also, observe in Table I that the path length increases with higher values of  $1 - \alpha$ . This is expected, as higher  $1 - \alpha$  typically results in non-singleton prediction sets, which produce a more conservative assignment of labels to cells, as discussed in Section III-B. Consequently, our planner generates longer paths to account for the most conservative labels. Similarly, since higher  $1 - \alpha$  often leads to non-singleton prediction sets, the proportion of the overall path spent on exploration is also higher for larger  $1 - \alpha$ .

### D. Comparative Experiments

**Baselines:** We compare our planner against the following baselines. (i) *Uncertainty-agnostic (UA) Planner:* This plan-

TABLE I  
COMPARATIVE EVALUATIONS

Framework	$1 - \alpha$ (%)	$S.R_{\text{map}}$ (%)	$S.R_{\text{mission}}$ (%)	Path length ( $m$ )	Exploration proportion (%)
Ours	95	93.36	98.36	74.7	19
	90	90.16	96.72	71.7	18.54
	85	86.89	95.08	69.72	11.2
UI	95	58.33	93.33	69.66	8.17
	90	41.67	76.67	66.14	4.65
	85	35	75	62.53	5.04
UA	NA	10.17	65.57	48.91	NA

ner assigns to each cell  $j$  the most-likely label as per the PMFs  $p_t(m_j)$ , i.e., the label assigned to cell  $j$  at time  $t$  is  $k_j = \text{argmax}_{k \in \mathcal{K}} p_t(m_j)$ . Using this label assignment, the planner employs  $A^*$  to compute paths that complete  $\psi$ . We select this baseline to illustrate the importance of designing planners that are aware of mapping uncertainty. (ii) *Uncertainty-informed (UI) Planner*: The second baseline differs from our planner only in the construction of prediction sets. Specifically, the predictions sets are built heuristically by treating the PMFs  $p_t(m_j)$  as true probabilities. Thus, the prediction sets are constructed as  $\mathcal{C}_j(\mathbf{m}_t) = \{\pi_1, \dots, \pi_k\}$ , where  $k = \sup \left\{ k' : \sum_{i=1}^{k'} p_t(m_j = \pi_i) < 1 - \alpha \right\} + 1$ , and  $\pi$  is the permutation of  $\mathcal{K}$  that sorts the classes from most likely to least likely, i.e.  $p_t(m_j = \pi_{n-1}) > p_t(m_j = \pi_n)$ . We select this baseline to illustrate the importance of calibrating uncertainty metrics provided by mapping algorithms.

**Comparative Results:** Table I shows the performance of both baselines using the evaluation metrics discussed in Section V-B. To ensure a fair comparison, both baselines are evaluated on the same 61 test scenarios used for our proposed method. Notice that the UI planner outperforms the UA planner in terms of mission and mapping success rates, as it accounts for mapping uncertainty. However, our method outperforms the UI baseline because the UI prediction sets—unlike ours—are constructed heuristically and are not supported by any correctness guarantees.

As seen in Table I, our approach leads to a significant improvement in both mapping and mission success rates. Our empirical evaluation shows that most baseline failures occur due to partial occlusions in the environment. An example is illustrated in Figure 4, where a human is partially occluded by trees. The cell associated with the human is often labeled as ‘tree’ by the UA planner, leading to safety violations because the human’ label has stricter safety constraints than the ‘tree’ label. In this case, by the time the UA planner detects the human, a safety constraint has already been violated. Similarly, the UI planner builds a singleton prediction set containing only the ‘tree’ label. In contrast, our approach constructs a prediction set that includes ‘tree’, ‘human’, and ‘free-space’, enabling the planner to follow a more conservative path and maintain safety. This results in higher mission and mapping success rates, though at the cost of longer paths, as shown in Table I.

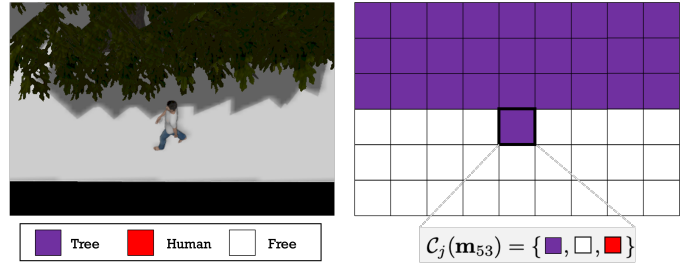


Fig. 4. Top view of the environment (left) and the corresponding 2D semantic map (right). The most likely label in  $\mathbf{m}_t$  for the cell  $j$  occupied by a human is ‘tree’. In contrast, the prediction set constructed by our method for that cell mitigates this mapping error by including ‘tree’, ‘human’, and ‘free-space’.

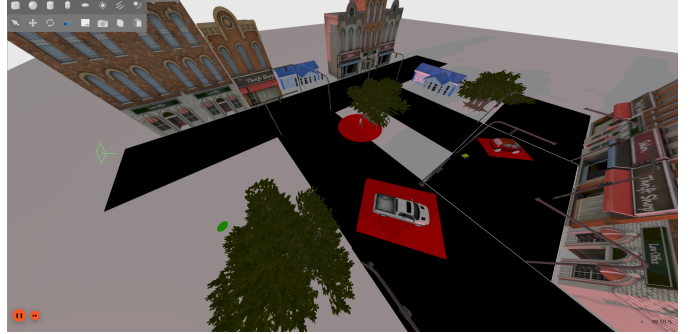


Fig. 5. Out-of-distribution environment with lighting that simulates dusk.

#### E. Evaluation in Out-of-Distribution Scenarios

Finally, we evaluated our method on out-of-distribution (OOD) environments where the position and the number of trees are randomized (instead of fixed when  $\mathcal{D}$  is used). We also changed the lighting conditions to simulate dawn and dusk. An example of an OOD environment is shown in Figure 5. For  $\alpha = 0.1$ , the empirical mapping success rates dropped to 80.33%, but the mission completion rate was met at 93.44%. As expected, this shows that the guarantees may no longer hold in OOD settings; see Section VI.

## VI. CONCLUSIONS AND FUTURE WORK

In this paper, we presented a novel semantic planner for unknown environments. Unlike related works, our method designs probabilistically correct paths in the presence of environmental uncertainty, stemming from imperfect perception, without any assumptions on sensor models or noise characteristics. The proposed method was supported both theoretically and experimentally. Future work will focus on: (i) designing active exploration algorithms that directly target reducing the size of prediction sets; (ii) accounting for OOD scenarios by leveraging robust CP methods; and (iii) directly quantifying sensor (rather than mapping) uncertainty.

## REFERENCES

- [1] P. Hart, N. Nilsson, and B. Raphael, “A formal basis for the heuristic determination of minimum cost paths,” *IEEE Transactions on Systems Science and Cybernetics*, vol. 4, no. 2, pp. 100–107, 1968.
- [2] S. Karaman and E. Frazzoli, “Sampling-based algorithms for optimal motion planning,” *The International Journal of Robotics Research*, vol. 30, no. 7, pp. 846–894, 2011.
- [3] L. Janson, E. Schmerling, A. Clark, and M. Pavone, “Fast marching tree: A fast marching sampling-based method for optimal motion planning in many dimensions,” *The International Journal of Robotics Research*, vol. 34, no. 7, pp. 883–921, 2015.

- [4] L. Gionfrida, C. Wang, L. Gan, M. Chli, and L. Carlone, "Computer and robot vision: Past, present, and future [TC spotlight]," *IEEE Robotics & Automation Magazine*, vol. 31, no. 3, pp. 211–215, 2024.
- [5] J. A. Placed, J. Strader, H. Carrillo, N. Atanasov, V. Indelman, L. Carlone, and J. A. Castellanos, "A survey on active simultaneous localization and mapping: State of the art and new frontiers," *IEEE Transactions on Robotics*, vol. 39, no. 3, pp. 1686–1705, 2023.
- [6] Y. Kantaros, S. Kalluraya, Q. Jin, and G. J. Pappas, "Perception-based temporal logic planning in uncertain semantic maps," *IEEE Transactions on Robotics*, vol. 38, no. 4, pp. 2536–2556, 2022.
- [7] J. Fu, N. Atanasov, U. Topcu, and G. J. Pappas, "Optimal temporal logic planning in probabilistic semantic maps," in *2016 IEEE International Conference on Robotics and Automation*, pp. 3690–3697.
- [8] M. Ryll, J. Ware, J. Carter, and N. Roy, "Semantic trajectory planning for long-distant unmanned aerial vehicle navigation in urban environments," in *2020 IEEE/RSJ International Conference on Intelligent Robots and Systems (IROS)*, pp. 1551–1558.
- [9] A. Ray, C. Bradley, L. Carlone, and N. Roy, "Task and motion planning in hierarchical 3d scene graphs," *arXiv preprint arXiv:2403.08094*, 2024.
- [10] J. G. Rogers and H. I. Christensen, "Robot planning with a semantic map," in *2013 IEEE International Conference on Robotics and Automation*, pp. 2239–2244.
- [11] E. Fahnstock, E. Fuentes, P. R. Osteen, S. Ancha, and N. Roy, "Learning semantic traversability priors using diffusion models for uncertainty-aware global path planning," in *ICRA 2024 Workshop on Resilient Off-road Autonomy*.
- [12] C. Galindo, J.-A. Fernández-Madriral, J. González, and A. Saffiotti, "Robot task planning using semantic maps," *Robotics and Autonomous Systems*, vol. 56, no. 11, pp. 955–966, 2008.
- [13] V. Vasilopoulos, G. Pavlakos, S. L. Bowman, J. D. Caporale, K. Daniilidis, G. J. Pappas, and D. E. Koditschek, "Reactive semantic planning in unexplored semantic environments using deep perceptual feedback," *IEEE Robotics and Automation Letters*, vol. 5, no. 3, pp. 4455–4462, 2020.
- [14] G. Malczyk, M. Kulkarni, and K. Alexis, "Semantically-driven deep reinforcement learning for inspection path planning," *IEEE Robotics and Automation Letters*, 2025.
- [15] G. Georgakis, B. Bucher, A. Arapin, K. Schmeckpeper, N. Matni, and K. Daniilidis, "Uncertainty-driven planner for exploration and navigation," in *2022 International Conference on Robotics and Automation (ICRA)*. IEEE, pp. 11 295–11 302.
- [16] A. Pal, Y. Qiu, and H. Christensen, "Learning hierarchical relationships for object-goal navigation," in *Conference on Robot Learning*. PMLR, 2021, pp. 517–528.
- [17] Z. Ravichandran, L. Peng, N. Hughes, J. D. Griffith, and L. Carlone, "Hierarchical representations and explicit memory: Learning effective navigation policies on 3d scene graphs using graph neural networks," in *IEEE International Conference on Robotics and Automation*, 2022, pp. 9272–9279.
- [18] S. L. Bowman, N. Atanasov, K. Daniilidis, and G. J. Pappas, "Probabilistic data association for semantic slam," in *IEEE International Conference on Robotics and Automation*, 2017, pp. 1722–1729.
- [19] A. Asgharivaskasi and N. Atanasov, "Semantic octree mapping and shannon mutual information computation for robot exploration," *IEEE Transactions on Robotics*, vol. 39, no. 3, pp. 1910–1928, 2023.
- [20] Y. Tian, Y. Chang, F. H. Arias, C. Nieto-Granda, J. P. How, and L. Carlone, "Kimera-multi: Robust, distributed, dense metric-semantic slam for multi-robot systems," *IEEE Transactions on Robotics*, vol. 38, no. 4, 2022.
- [21] E. Psomiadis and P. Tsiotras, "HCOA\*: Hierarchical class-ordered a\* for navigation in semantic environments," *arXiv preprint arXiv:2505.03128*, 2025.
- [22] J. Wilson, R. Xu, Y. Sun, P. Ewen, M. Zhu, K. Barton, and M. Ghaffari, "Latentbki: Open-dictionary continuous mapping in visual-language latent spaces with quantifiable uncertainty," *IEEE Robotics and Automation Letters*, vol. 10, no. 4, pp. 3102–3109, 2025.
- [23] V. Renganathan, I. Shames, and T. H. Summers, "Towards integrated perception and motion planning with distributionally robust risk constraints," *IFAC-PapersOnLine*, vol. 53, no. 2, pp. 15 530–15 536, 2020.
- [24] V. Renganathan, S. Safaoui, A. Kothari, B. Gravell, I. Shames, and T. Summers, "Risk bounded nonlinear robot motion planning with integrated perception & control," *Artificial Intelligence*, vol. 314, p. 103812, 2023.
- [25] A. Bry and N. Roy, "Rapidly-exploring random belief trees for motion planning under uncertainty," in *2011 IEEE international conference on robotics and automation*, pp. 723–730.
- [26] L. Palmieri, T. P. Kucner, M. Magnusson, A. J. Lilienthal, and K. O. Arras, "Kinodynamic motion planning on gaussian mixture fields," in *2017 IEEE International Conference on Robotics and Automation (ICRA)*, pp. 6176–6181.
- [27] Q. H. Ho, Z. N. Sunberg, and M. Lahijanian, "Gaussian belief trees for chance constrained asymptotically optimal motion planning," in *2022 International Conference on Robotics and Automation (ICRA)*. IEEE, pp. 11 029–11 035.
- [28] M. Minderer, J. Djolonga, R. Romijnders, F. Hubis, X. Zhai, N. Houlsby, D. Tran, and M. Lucic, "Revisiting the calibration of modern neural networks," *Advances in Neural Information Processing Systems*, vol. 34, pp. 15 682–15 694, 2021.
- [29] A. N. Angelopoulos and S. Bates, "A gentle introduction to conformal prediction and distribution-free uncertainty quantification," 2022.
- [30] A. Dixit, Z. Mei, M. Booker, M. Storey-Matsutani, A. Z. Ren, and A. Majumdar, "Perceive with confidence: Statistical safety assurances for navigation with learning-based perception," in *arXiv preprint arXiv:2403.08185*, 2023.
- [31] L. Lindemann, Y. Zhao, X. Yu, G. J. Pappas, and J. V. Deshmukh, "Formal verification and control with conformal prediction," *arXiv preprint arXiv:2409.00536*, 2024.
- [32] L. Lindemann, M. Cleaveland, G. Shim, and G. J. Pappas, "Safe planning in dynamic environments using conformal prediction," *IEEE Robotics and Automation Letters*, 2023.
- [33] S. Sheng, P. Yu, D. Parker, M. Kwiatkowska, and L. Feng, "Safe pomdp online planning among dynamic agents via adaptive conformal prediction," *IEEE Robotics and Automation Letters*, 2024.
- [34] A. Z. Ren, A. Dixit, A. Bodrova, S. Singh, S. Tu, N. Brown, P. Xu, L. Takayama, F. Xia, J. Varley *et al.*, "Robots that ask for help: Uncertainty alignment for large language model planners," *arXiv preprint arXiv:2307.01928*, 2023.
- [35] J. Wang, G. He, and Y. Kantaros, "Probabilistically correct language-based multi-robot planning using conformal prediction," *IEEE Robotics and Automation Letters*, 2024.
- [36] J. Lekeufack, A. N. Angelopoulos, A. Bajcsy, M. I. Jordan, and J. Malik, "Conformal decision theory: Safe autonomous decisions from imperfect predictions," in *2024 IEEE International Conference on Robotics and Automation (ICRA)*, pp. 11 668–11 675.
- [37] A. Angelopoulos, S. Bates, J. Malik, and M. I. Jordan, "Uncertainty sets for image classifiers using conformal prediction," *arXiv preprint arXiv:2009.14193*, 2020.
- [38] J. Sun, Y. Jiang, J. Qiu, P. Nobel, M. J. Kochenderfer, and M. Schwager, "Conformal prediction for uncertainty-aware planning with diffusion dynamics model," *Advances in Neural Information Processing Systems*, vol. 36, pp. 80 324–80 337, 2023.
- [39] H. Zhang and L. Carlone, "Champ: Conformalized 3d human multi-hypothesis pose estimators," *arXiv preprint arXiv:2407.06141*, 2024.
- [40] A. Milioto and C. Stachniss, "Bonnet: An open-source training and deployment framework for semantic segmentation in robotics using cnns," in *2019 International Conference on Robotics and Automation (ICRA)*. IEEE, pp. 7094–7100.
- [41] R. P. de Figueiredo, J. le Fevre Sejersen, J. G. Hansen, M. Brandão, and E. Kayacan, "Real-time volumetric-semantic exploration and mapping: An uncertainty-aware approach," in *IEEE/RSJ International Conference on Intelligent Robots and Systems*, 2021, pp. 9064–9070.
- [42] A. N. Angelopoulos and S. Bates, "Conformal prediction: A gentle introduction," *Foundations and Trends in Machine Learning*, vol. 16, no. 4, pp. 494–591, 2023.
- [43] V. Vovk, "Conditional validity of inductive conformal predictors," in *Asian conference on machine learning*. PMLR, 2012, pp. 475–490.
- [44] Demonstrations, <https://vimeo.com/1122929308?share=copy>.
- [45] S. Macenski, T. Foote, B. Gerkey, C. Lalancette, and W. Woodall, "Robot operating system 2: Design, architecture, and uses in the wild," *Science Robotics*, vol. 7, no. 66, p. eabm6074, 2022.
- [46] Y. Wu, A. Kirillov, F. Massa, W.-Y. Lo, and R. Girshick, "Detectron2," 2019.
- [47] T. Lin, M. Maire, S. J. Belongie, L. D. Bourdev, R. B. Girshick, J. Hays, P. Perona, D. Ramanan, P. Dollár, and C. L. Zitnick, "Microsoft COCO: common objects in context," *CORR*, vol. abs/1405.0312, 2014.